Donor-Acceptor-Donor Molecules for High Performance Near Ultraviolet Organic Light-Emitting Diodes via Hybridized Local and Charge-Transfer Process

Xianhui Wang,[a,‡] Zhangshan Liu,[b,‡] Sinuo Geng,[a] Ziting Zhong,[a] Huihui Li,[a] Xin Jiang Feng,*[,a] Zujin Zhao,*[,b] and Hua Lu*[,a]

I. Supplementary Figures, Scheme and Tables.

1. **Fig. S1**. Natural transition orbitals of S_0 to $S_{1/2}$ and S_0 to $T_{1/8/9}$ for 5,10-CzPPI and 6,9-CzPPI................................S2
2. **Fig. S2**. Hole (blue) and electron (green) distribution of transitions for 5,10-CzPPI and 6,9-CzPPI.................S2
3. **Scheme S1**. Synthetic routes for 5,10-CzPPI and 6,9-CzPPI..S3
4. **Fig. S3**. TGA and DSC (inset) traces of 5,10-CzPPI and 6,9-CzPPI..S4
5. **Table S1**. Photophysical properties of 5,10-CzPPI and 6,9-CzPPI in different solvents...S4
6. **Fig. S4**. Lippert-Mataga plots of Stokes shifts versa solvent polarizabilties for 5,10-CzPPI and 6,9-CzPPI............S5
7. **Fig. S5**.Transient PL spectra of 5,10-CzPPI and 6,9-CzPPI in dichloromethane and in thin films..........................S5
8. **Fig. S6**. Cyclic voltammograms for 5,10-CzPPI and 6,9-CzPPI...S5
9. **Table S2**. Electronic excitation energies, oscillator strengths and MO transition contributions……………………S6
10. **Fig. S7**. Electroluminescence properties of the devices based on 5,10-CzPPI……………………………………S7
11. **Fig. S8**. Electroluminescence properties of the devices based on 6,9-CzPPI...S7

II. Measurements..S8

III. ^{1}H NMR of **5,10-CzPPI** and **6,9-CzPPI** in $CDCl_3$ or CD_2Cl_2..S11

IV. ^{13}C NMR of **5,10-CzPPI** and **6,9-CzPPI** in $CDCl_3$ or CD_2Cl_2...S14

V. HR-MS of **5,10-CzPPI** and **6,9-CzPPI**..S16

I. Supplementary Figures, Scheme and Tables

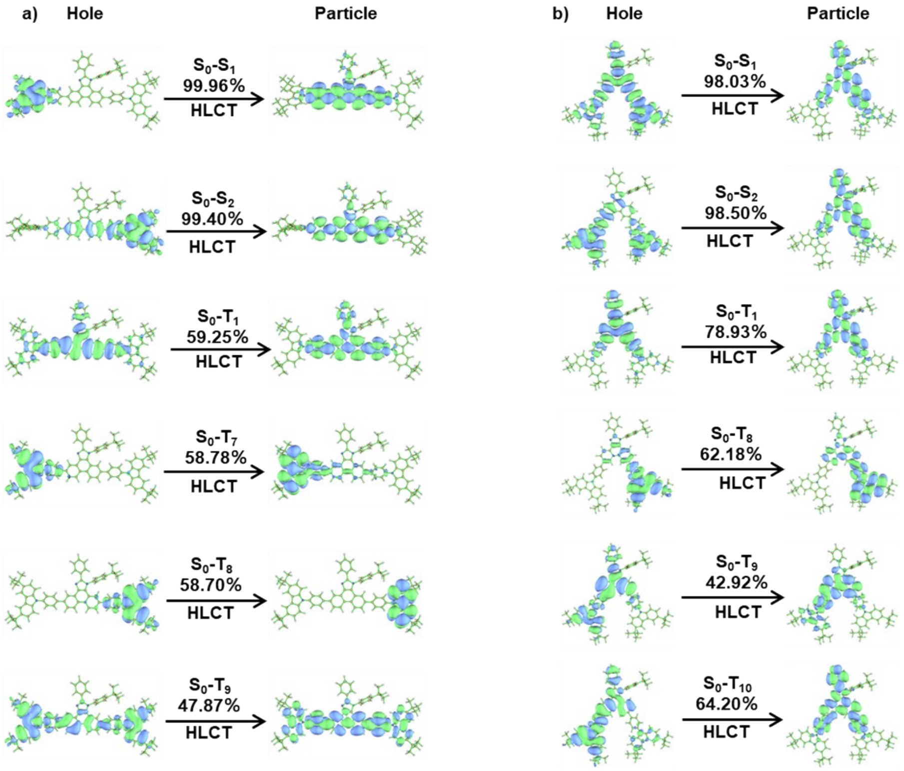

Fig. S1. Natural transition orbitals of S_0 to $S_{1/2}$ and S_0 to $T_{17//8/9/10}$ for 5,10-CzPPI and 6,9-CzPPI.

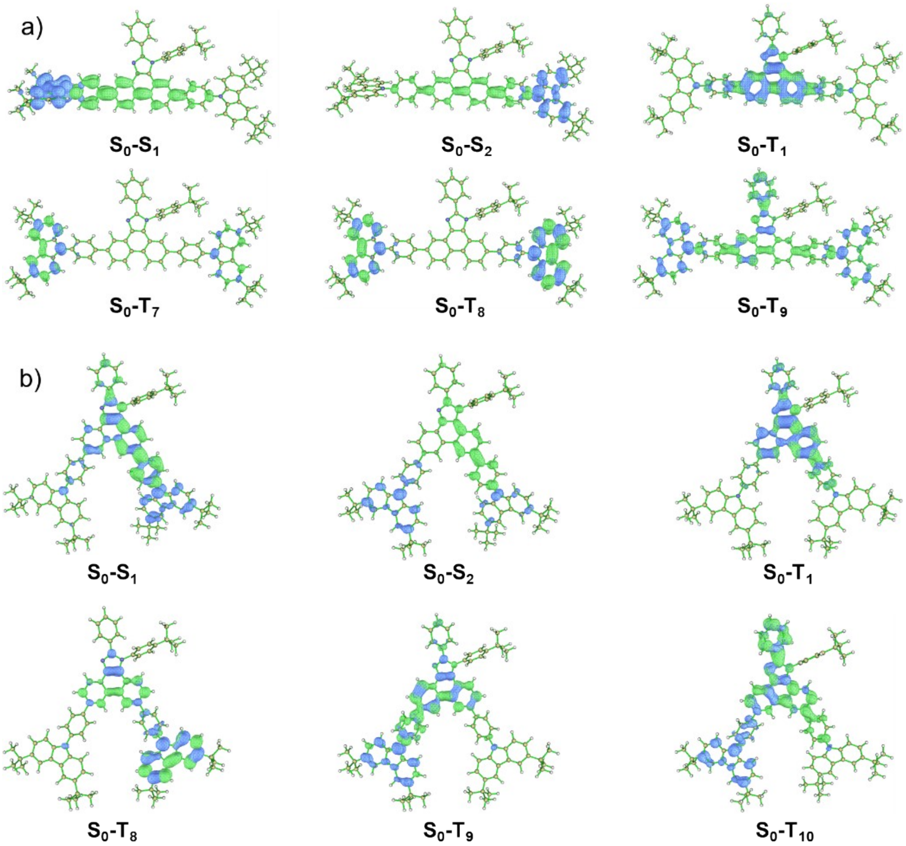

Fig. S2. Isosurface of the hole (blue) and electron (green) distribution calculated by Multiwfn 3.8(dev) of S_0 to $S_{1/2}$ and S_0 to $T_{1/7//8/9/10}$ for 5,10-CzPPI and 6,9-CzPPI.

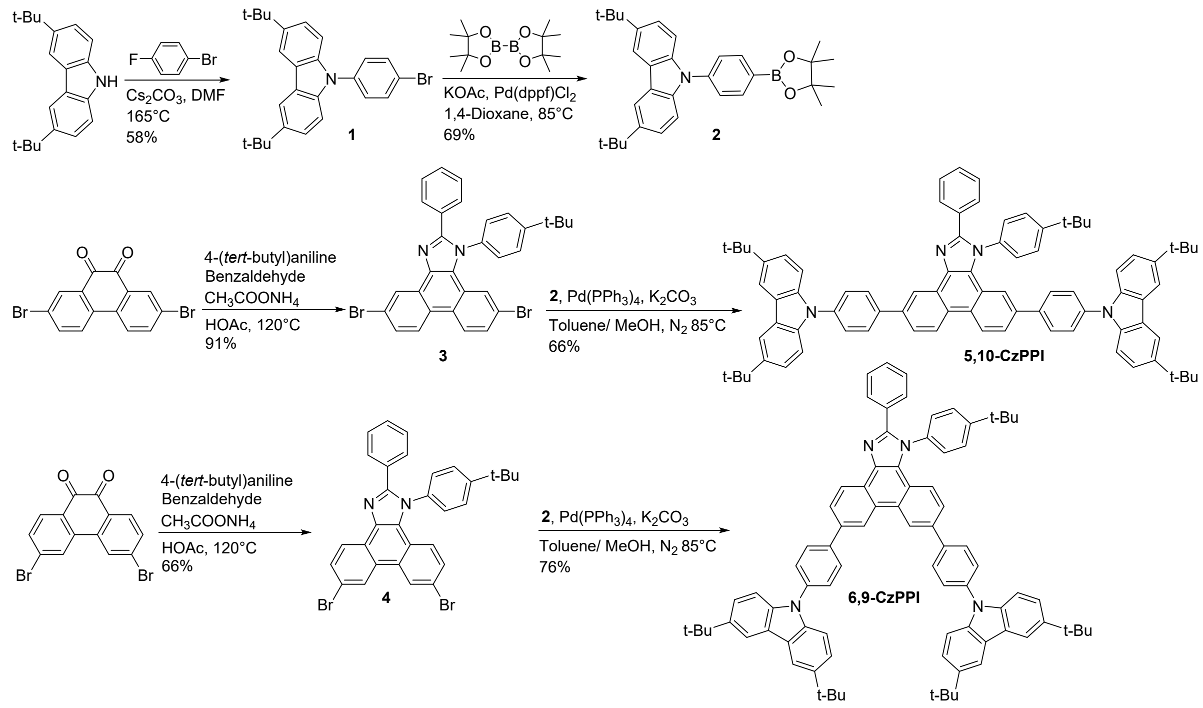

Scheme S1. Synthetic routes for 5,10-CzPPI and 6,9-CzPPI.

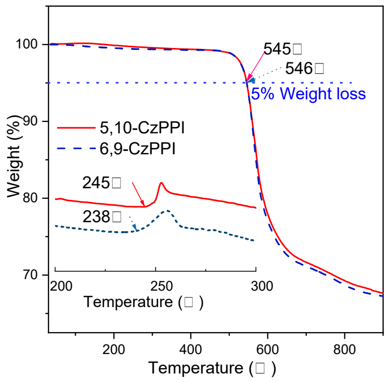

Fig. S3. TGA and DSC (inset) traces of 5,10-CzPPI and 6,9-CzPPI.

Table S1. Photophysical properties of 5,10-CzPPI and 6,9-CzPPI in different solvents.

	Solvent	λ_{abs} [a] (nm)	λ_{em} [b] (nm)	$\Delta\nu_{em-abs}$ [c] (cm^{-1})	Φ_F [d]	τ(ns) [e]	k_r [f]	k_{nr} [f]
5,10-CzPPI	hexane	349	400	3653	0.352	6.6	0.053	0.098
	toluene	350	406	3941	0.449	nd	nd	nd
	ethyl ether	348	403	3922	0.426	8.3	0.051	0.083
	benzene	352	405	3718	0.538	-	-	-
	DCM	350	413	4358	0.564	8.2	0.069	0.053
	THF	349	412	4381	0.463	9.0	0.051	0.060
	EA	349	410	4262	0.435	8.6	0.050	0.066
	dioxane	350	411	4241	0.574	10.2	0.056	0.042
	TEA	349	403	3839	0.105	nd	nd	nd
	ACN	348	430	5480	0.552	4.2	0.131	0.150
	DMF	351	432	5342	0.655	6.8	0.096	0.051
	DMSO	352	438	5578	-	6.7	-	-
6,9-CzPPI	hexane	333	390	4389	0.593	3.5	0.424	0.116
	toluene	336	394	4381	0.379	1.8	0.211	0.345
	ethyl ether	332	391	4545	0.652	4.2	0.155	0.083
	benzene	335	395	4534	0.755	9.7	0.078	0.025
	DCM	335	397	4662	0.636	4.4	0.145	0.083
	THF	334	394	4559	0.445	4.0	0.111	0.139
	EA	334	392	4430	0.638	4.1	0.156	0.088
	dioxane	335	394	4470	0.771	3.7	0.208	0.062
	TEA	335	391	4275	0.182	nd	nd	nd
	ACN	332	396	4868	0.552	4.2	0.131	0.107
	DMF	334	397	4751	0.474	3.5	0.135	0.150
	DMSO	337	400	4674	-	3.6		

[a] Absorption maxima. [b] Emission maxima. [c] Stokes-shift value. [d] Fluorescence quantum yields. [e] Fluorescence lifetime detected at the maximum fluorescence wavelengths (nd = not detected; Lifetimes or fluorescence quantum yields in benzene and DMSO haven't been measured). [f] Constants of radiative transition and nonradiative transition.

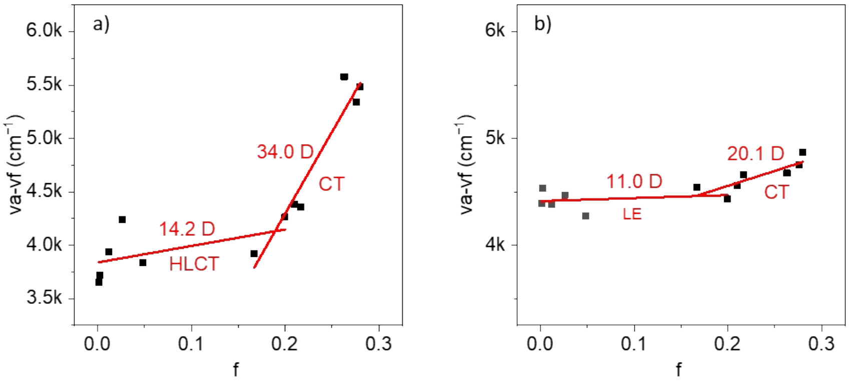

Fig. S4. Lippert-Mataga plots of Stokes shifts versa solvent polarizabilties for a) 5,10-CzPPI and b) 6,9-CzPPI.

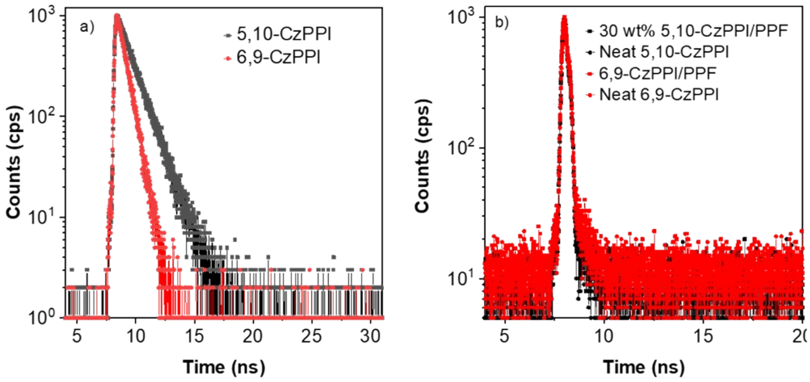

Fig. S5.Transient PL spectra of 5,10-CzPPI and 6,9-CzPPI in dichloromethane a) and in thin films b).

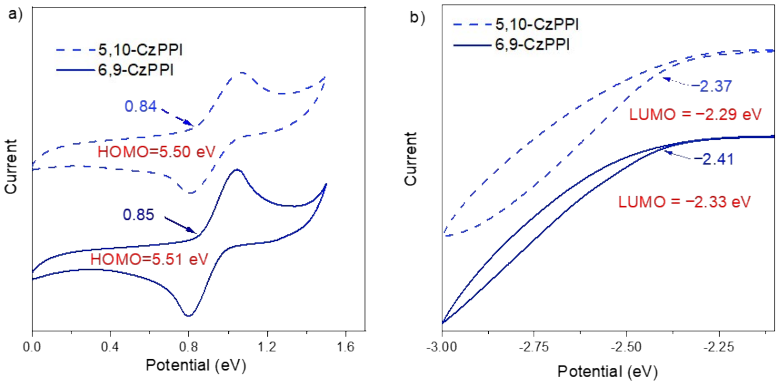

Fig. S6. Cyclic voltammograms (CV) and differential pulse voltammetry (DPV) curves of 5,10-CzPPI and 6,9-CzPPI using Ag/Ag$^+$ as a reference electrode measured in CH_2Cl_2. The onset potential for oxidative curve of ferrocene is 0.14 V.

Table S2. Calculated electronic excitation energies, oscillator strengths and MO transition contributions for 5,10-CzPPI and 6,9-CzPPI using the B3LYP functional with the 6-31G(d,p) basis set.

Compound	State[a]	Energy (eV)	λ (nm)	*f* [b]	Wave function [c]
5,10-CzPPI	S_1	3.26	380	0.707	H→L (92%)
	S_2	3.38	368	0.1361	H−2→L (58%), H−1→L (32%)
	S_3	3.41	364	0.1156	H−2→L (28%), H−1→L (59%)
	S_4	3.71	335	0.0629	H→L+1 (88%)
	S_5	3.78	328	0.1176	H−5→L (29%), H−2→L+1 (57%)
	S_8	3.90	318	0.2818	H−1→L+3 (15%), H→L+6 (65%)
	S_9	3.91	318	0.0647	H−1→L+3 (62%), H→L+6 (23%)
	S_{10}	3.94	315	0.3279	H−5→L (37%), H−2→L+1 (17%), H−2→L+2 (21%), H−1→L+3 (10%)
6,9-CzPPI	S_1	3.32	375	0.5556	H−1→L (18%), H→L (74%)
	S_2	3.46	359	0.1777	H−1→L (76%), H→L (16%)
	S_3	3.54	351	0.3772	H−2→L+1 (11%), H→L+1 (70%)
	S_4	3.65	340	0.2197	H−2→L (79%), H→L+2 (11%)
	S_5	3.67	339	0.1906	H−2→L (11%), H−1→L+1 (13%), H→L+2 (43%)
	S_8	3.90	318	0.1565	H−2→L+1 (14%), H−1→L+6 (10%), H→L+3 (23%), H→L+6 (30%)
	S_9	3.90	318	0.0543	H−1→L+4 (50%), H→L+4 (22%)

[a] Excited state. [b] Oscillator strength (values < 0.05 are not included). [c] MOs involved in the transitions, H = HOMO, L = LUMO.

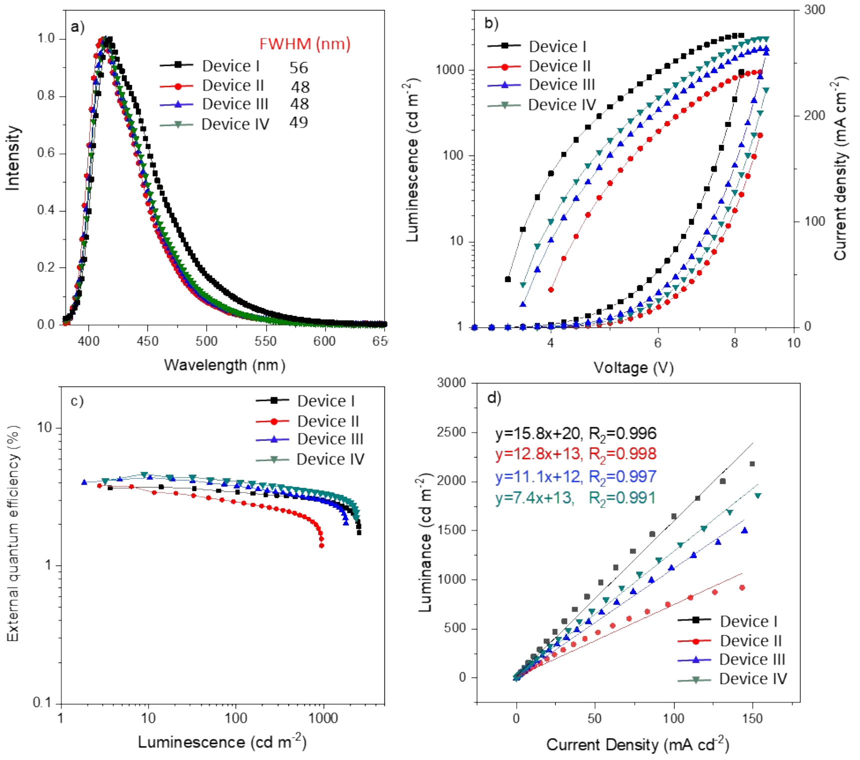

Fig. S7. a) EL spectra, b) luminance-voltage-current density c) external quantum efficiency-luminance and d) luminance vs current density (symbol) and the fitted curve plot (line) of devices characteristics of the devices based on 5,10-CzPPI.

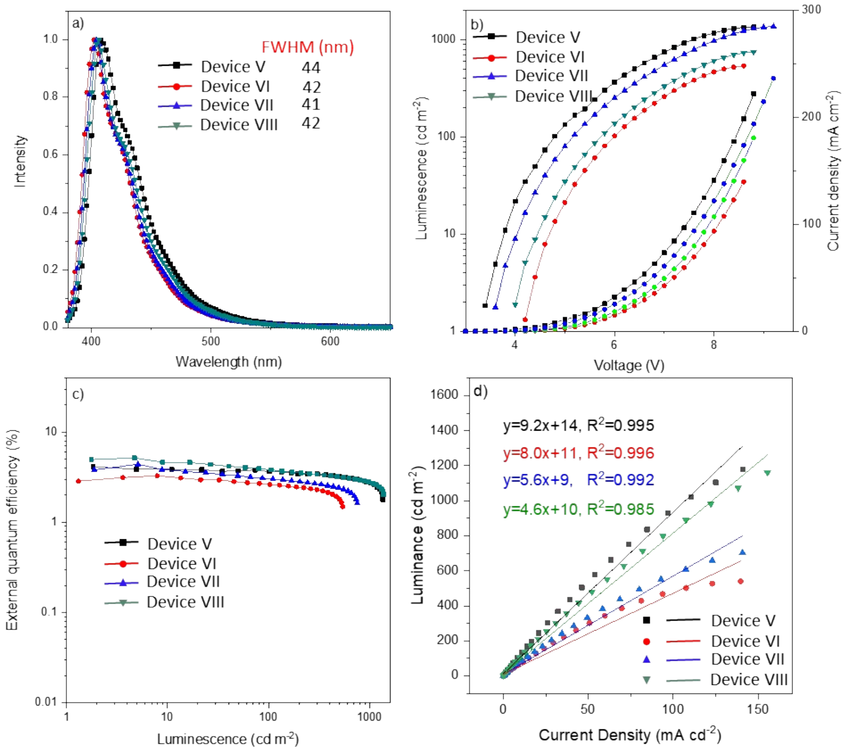

Fig. S8. a) EL spectra, b) luminance-voltage-current density c) external quantum efficiency-luminance and d) luminance vs current density (symbol) and the fitted curve plot (line) of devices characteristics of the devices based on 6,9-CzPPI.

II. Measurements

Photophysical, thermal and electrochemical property measurements.

All reagents and solvents were used as purchased from commercial sources. Toluene and tetrahydrofuran were anhydrous. ^{1}H NMR and ^{13}C NMR spectra, mass spectrometric measurements, thermogravimetric analysis, differential scanning calorimetry (DSC) analysis, UV-Vis spectra, and fluorescence spectra in solution were measured using a Bruker AM 400/500 spectrometer, MicroQII mass spectrometer, TGA instrument (PE-TGA6), TA Instruments DSC 2920, Shimadzu UV-1800 spectrophotometer and Horiba JobinYvon Fluorolog-3 spectrofluorimeter, respectively. The fluorescence quantum yields were measured by the integrating sphere using Hamamatsu C13534 spectrometer under air atmosphere. Cyclic voltammetric (CV) measurements were carried out in a conventional three-electrode cell, using a Pt button working electrode, a platinum wire counter electrode, and an Ag/$AgNO_3$ reference electrode using a computer-controlled CHI650E at room temperature in dichloromethane containing Bu_4NPF_6 (0.1 M) as the supporting electrolyte. The electroluminescence spectra, current density, and luminance were tested using an Ocean Optics USB 2000 spectrometer, dual-channel Keithley 2614B source meter and PIN-25D silicon photodiode, respectively.

Lippert-Mataga analysis.

Lippert-Mataga analysis was performed to estimate the magnitude of the excited state dipole moment of 5,10-CzPPI and 6,9-CzPPI. The energy difference of the fluorescence maximum relative to the absorption maximum as a function of the solvent orientation parameter (Δf) has been used as a measure of the change in dipole moment between the excited state and the ground state. Based on the Lippert–Mataga equation 1, the difference between the dipole moment of the excited and ground state ($\Delta\mu$) can be estimated from the slope of a plot of $\Delta\nu$ versus Δf:

$$\Delta\nu = \nu_a - \nu_f = \frac{1}{4\pi\varepsilon_0 hca^3}\frac{2\Delta\mu^2}{}\Delta f + constant \qquad (1)$$

where $\Delta\nu$ is the Stokes shift (in wavenumber), ε_0 is the dielectric constant of a vacuum, h is Planck's constant, c is the speed of light, a is the radius of the Onsager cavity, and Δf is the orientational polarizability of the solvent, defined as follows:

$$\Delta f = \frac{\varepsilon - 1}{2\varepsilon + 1} - \frac{n^2 - 1}{2n^2 - 1} \qquad (2)$$

where ε and n are the dielectric constant and the refractive index of the solvent, respectively.

The calculated α values are 8.21 Å and 8.60 Å for 5,10-CzPPI and 6,9-CzPPI, respectively, using the B3LYP/6-31G (d) method. The $\Delta\mu$ value are 7.7 D and 31.2 D estimated from the slope of the Lippert–Mataga plot for 5,10-CzPPI in low polarity region and high polarity region, respectively. Accordingly, the μ_e values are estimated to be 14.2 D in low polarity solvents and 34.0 D in in high polarity solvents for 5,10-CzPPI. Similarly, the μ_e values 6,9-CzPPI are calculated to be 11.0 D and 20.1 D from $\Delta\mu$ (1.1 and 20.2 D) in solvents.

Device fabrication and EL performance measurements.

Glass substrates pre-coated with a 90 nm-thin layer of indium tin oxide (ITO) with a sheet resistance of 15-20 Ω per square were thoroughly cleaned for 10 minutes in ultrasonic bath of acetone, isopropyl alcohol, detergent, deionized water, and isopropyl alcohol and then treated with O_2 plasma for 10 min in sequence. All of the organic materials used were purified by a vacuum sublimation approach. Organic layers were deposited onto the ITO-coated substrates by high-vacuum ($< 5\times 10^{-4}$ Pa) thermal evaporation. Deposition rates were controlled by independent quartz crystal oscillators, which are 1~2 Å s^{-1} for organic materials, 0.1 Å s^{-1} for LiF, and 5 Å s^{-1} for Al, respectively. The emission area of the devices is 3 mm × 3 mm as shaped by the overlapping area of the anode and cathode. All the device characterization steps were carried out at room temperature under ambient laboratory conditions without encapsulation. EL spectra were taken by normal direction utilizing a spectrometer (Ocean Optics USB 2000+). Luminance−voltages− current density characteristics were measured by a Konica Minolta CS-200 Color and Luminance Mete, along with a Keithley 2400 Source Meter. The external quantum efficiencies were estimated utilizing the normalized EL spectra and the current efficiencies of the devices, assuming that the devices are Lambertian emitters.

III. ^{1}H NMR spectra of compounds

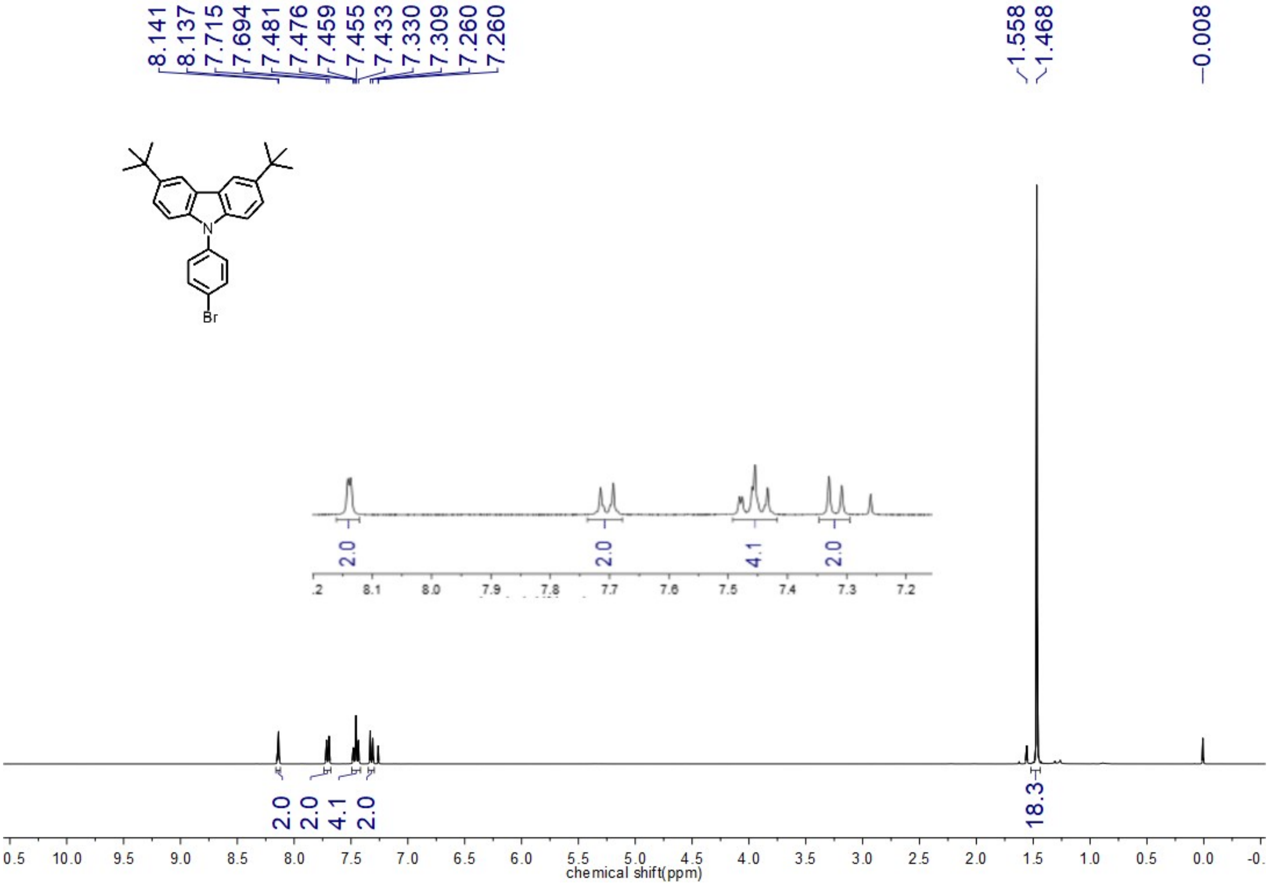

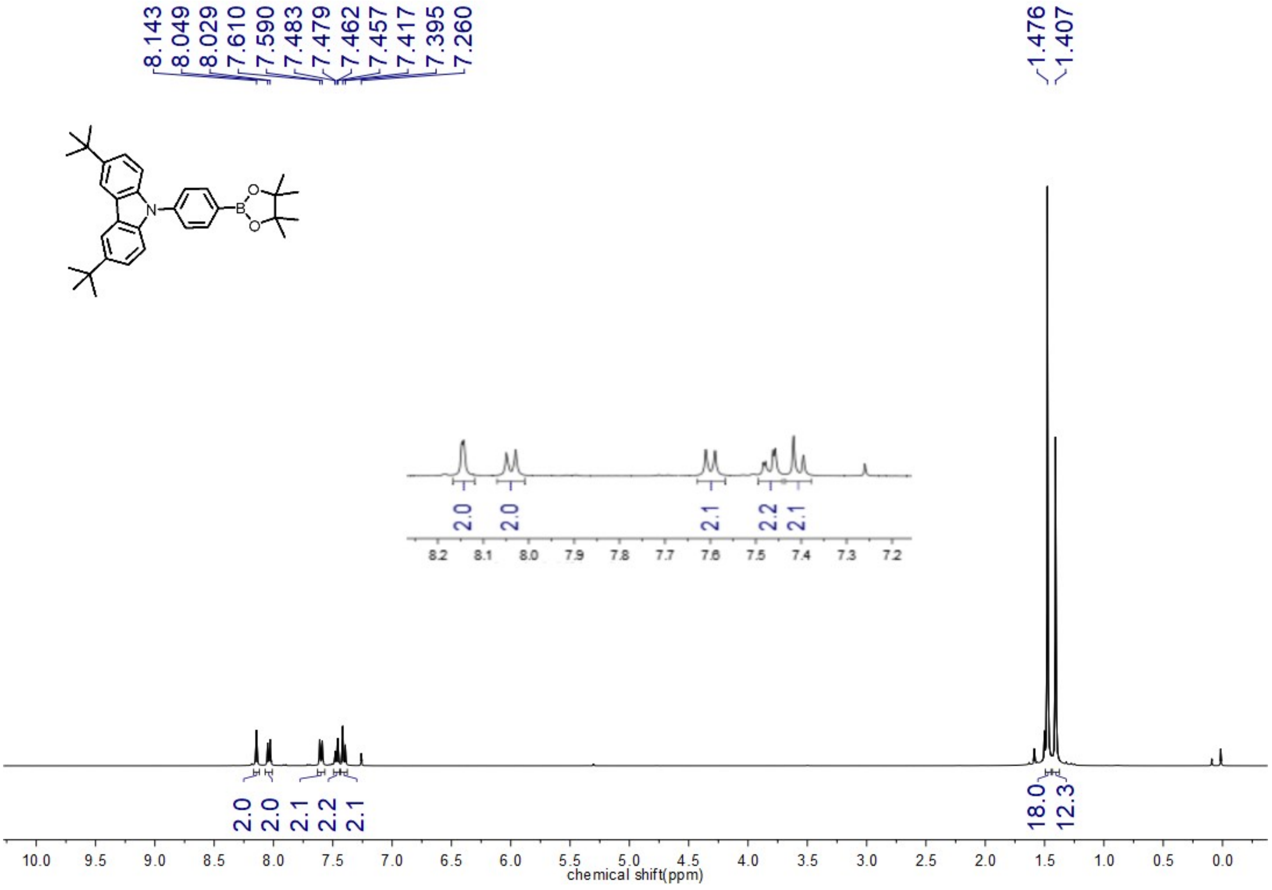

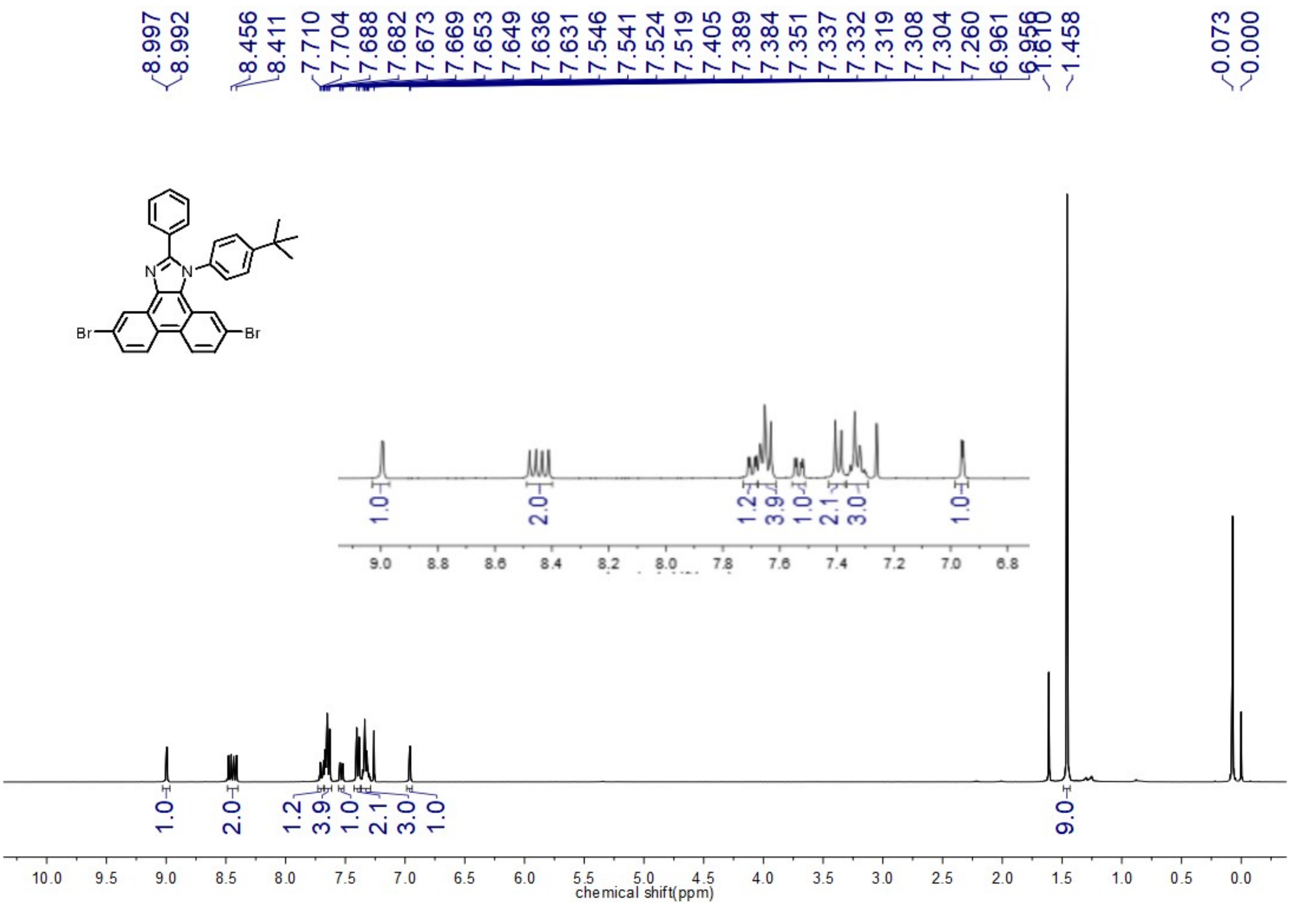
8.997
8.992
8.456
8.411
7.710
7.704
7.688
7.682
7.673
7.669
7.653
7.649
7.636
7.631
7.546
7.541
7.524
7.519
7.405
7.389
7.384
7.351
7.337
7.332
7.319
7.308
7.304
7.260
6.961
6.956
1.610
1.458
0.073
0.000
Br
Br
N
N
1.0
2.0
1.2
3.9
1.0
2.1
3.0
1.0
9.0
9.0
8.8
8.6
8.4
8.2
8.0
7.8
7.6
7.4
7.2
7.0
6.8
10.0
9.5
9.0
8.5
8.0
7.5
7.0
6.5
6.0
5.5
5.0
4.5
4.0
3.5
3.0
2.5
2.0
1.5
1.0
0.5
0.0
chemical shift(ppm)

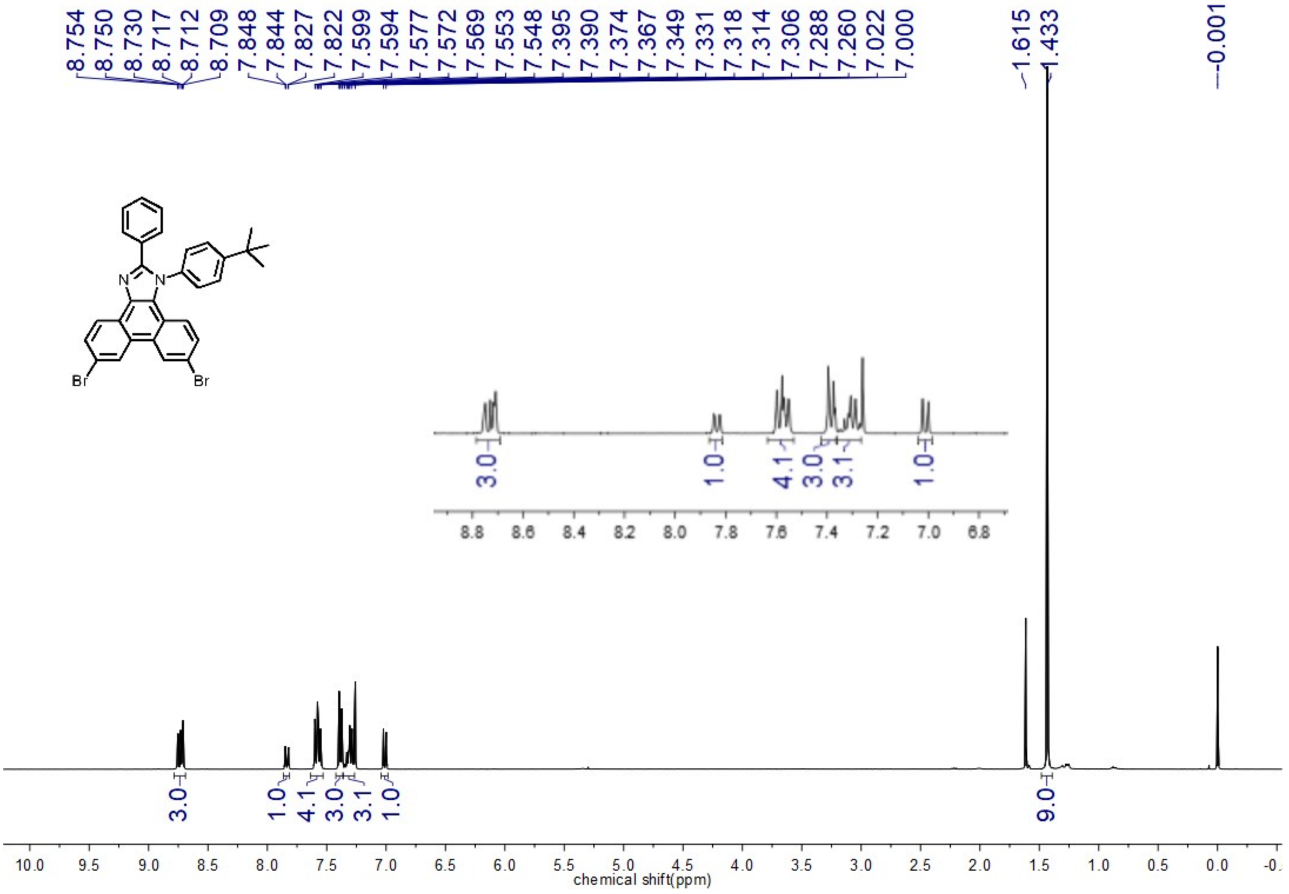
8.754
8.750
8.730
8.717
8.712
8.709
7.848
7.844
7.827
7.822
7.599
7.594
7.577
7.572
7.569
7.553
7.548
7.395
7.390
7.374
7.367
7.349
7.331
7.318
7.314
7.306
7.288
7.260
7.022
7.000
1.615
1.433
-0.001
Br
Br
N
N
3.0
1.0
4.1
3.0
3.1
1.0
9.0
8.8
8.6
8.4
8.2
8.0
7.8
7.6
7.4
7.2
7.0
6.8
10.0
9.5
9.0
8.5
8.0
7.5
7.0
6.5
6.0
5.5
5.0
4.5
4.0
3.5
3.0
2.5
2.0
1.5
1.0
0.5
0.0
-0.
chemical shift(ppm)

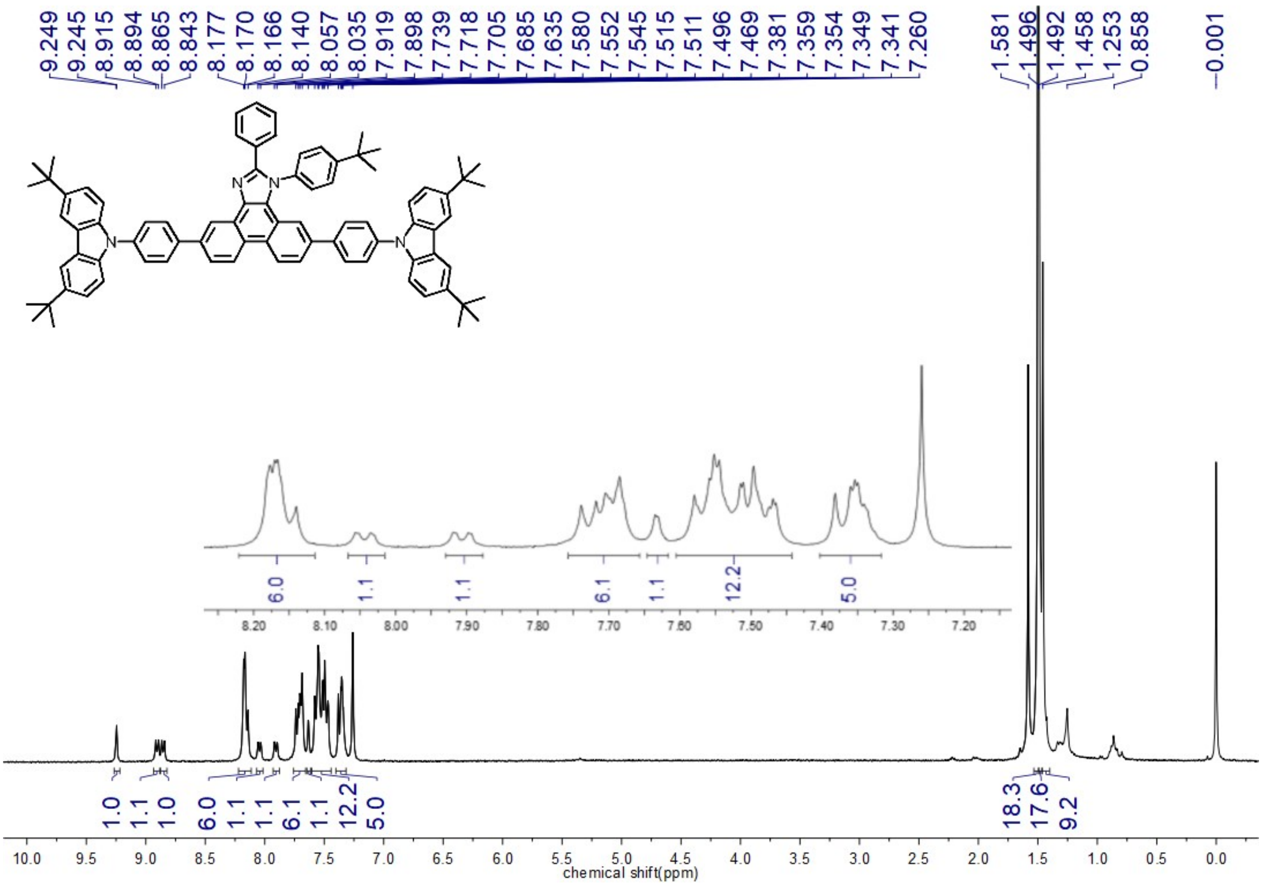
9.249
9.245
8.915
8.894
8.865
8.843
8.177
8.170
8.166
8.140
8.057
8.035
7.919
7.898
7.739
7.718
7.705
7.685
7.635
7.580
7.552
7.545
7.515
7.511
7.496
7.469
7.381
7.359
7.354
7.349
7.341
7.260
1.581
1.496
1.492
1.458
1.253
0.858
-0.001
N
N
N
N
6.0
1.1
1.1
6.1
1.1
12.2
5.0
8.20
8.10
8.00
7.90
7.80
7.70
7.60
7.50
7.40
7.30
7.20
1.0
1.1
1.0
6.0
1.1
1.1
6.1
1.1
12.2
5.0
18.3
17.6
9.2
10.0
9.5
9.0
8.5
8.0
7.5
7.0
6.5
6.0
5.5
5.0
4.5
4.0
3.5
3.0
2.5
2.0
1.5
1.0
0.5
0.0
chemical shift(ppm)

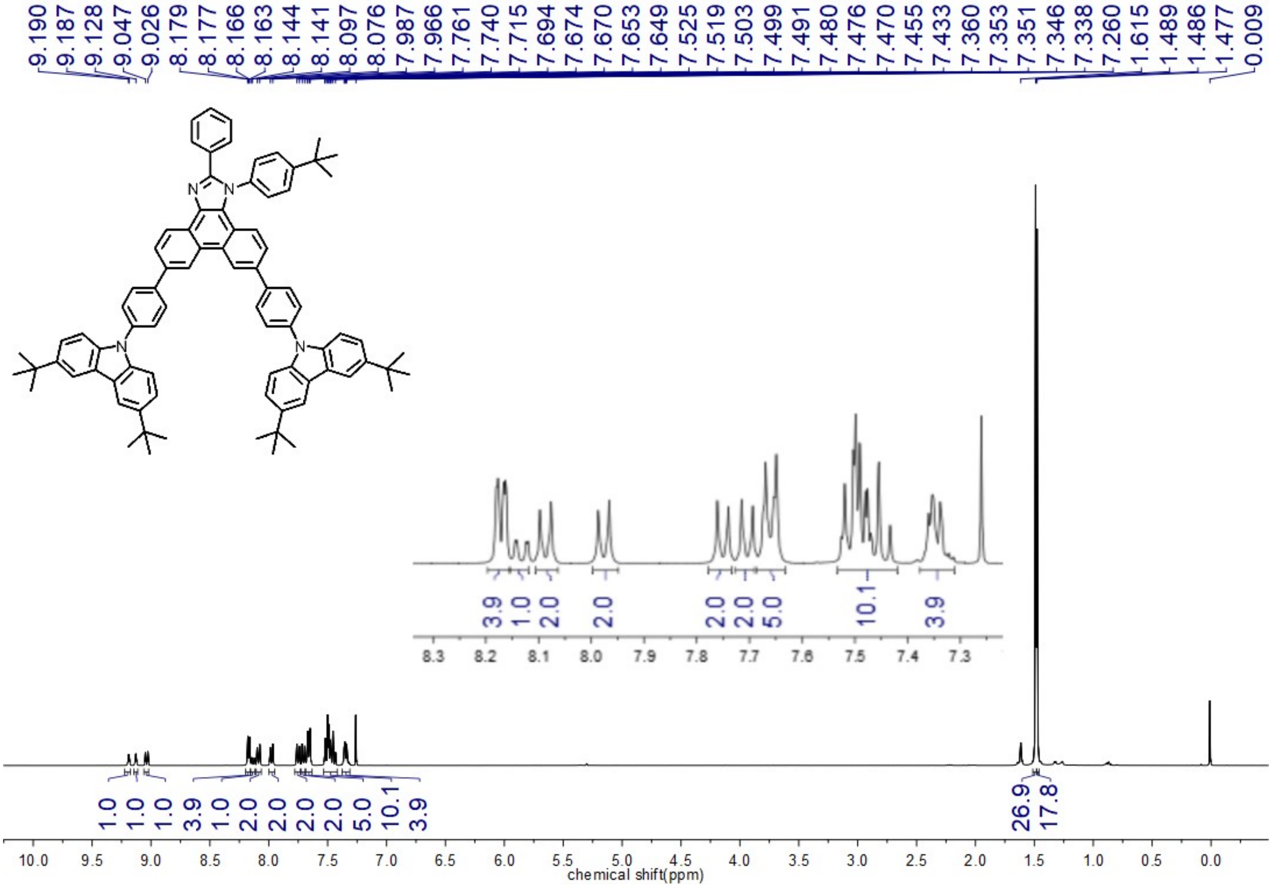
9.190
9.187
9.128
9.047
9.026
8.179
8.177
8.166
8.163
8.144
8.141
8.097
8.076
7.987
7.966
7.761
7.740
7.715
7.694
7.674
7.670
7.653
7.649
7.525
7.519
7.503
7.499
7.491
7.480
7.476
7.470
7.455
7.433
7.360
7.353
7.351
7.346
7.338
7.260
1.615
1.489
1.486
1.477
0.009
N
N
N
N
3.9
1.0
2.0
2.0
2.0
2.0
5.0
10.1
3.9
8.3
8.2
8.1
8.0
7.9
7.8
7.7
7.6
7.5
7.4
7.3
1.0
1.0
1.0
3.9
1.0
2.0
2.0
2.0
2.0
5.0
10.1
3.9
26.9
17.8
10.0
9.5
9.0
8.5
8.0
7.5
7.0
6.5
6.0
5.5
5.0
4.5
4.0
3.5
3.0
2.5
2.0
1.5
1.0
0.5
0.0
chemical shift(ppm)

IV. ^{13}C NMR spectra of compounds

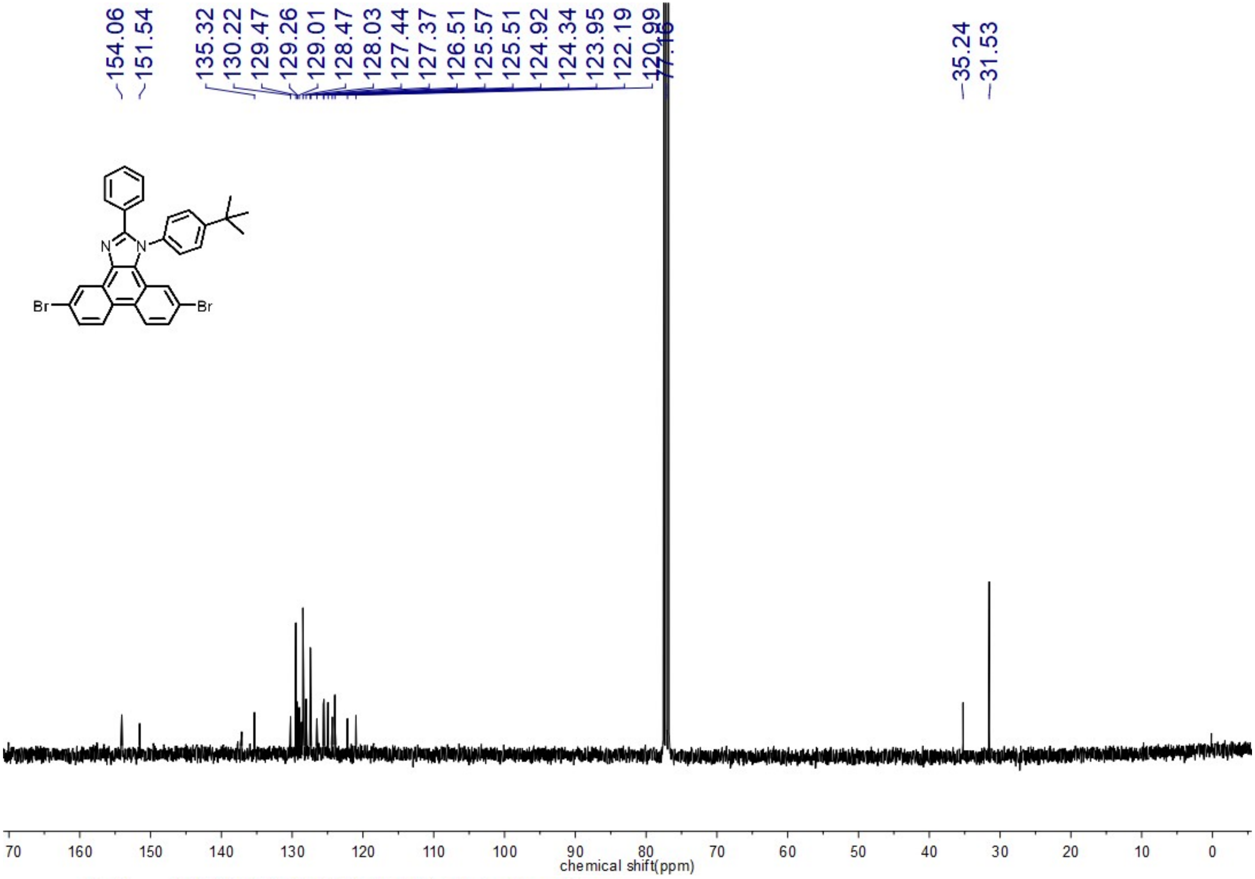

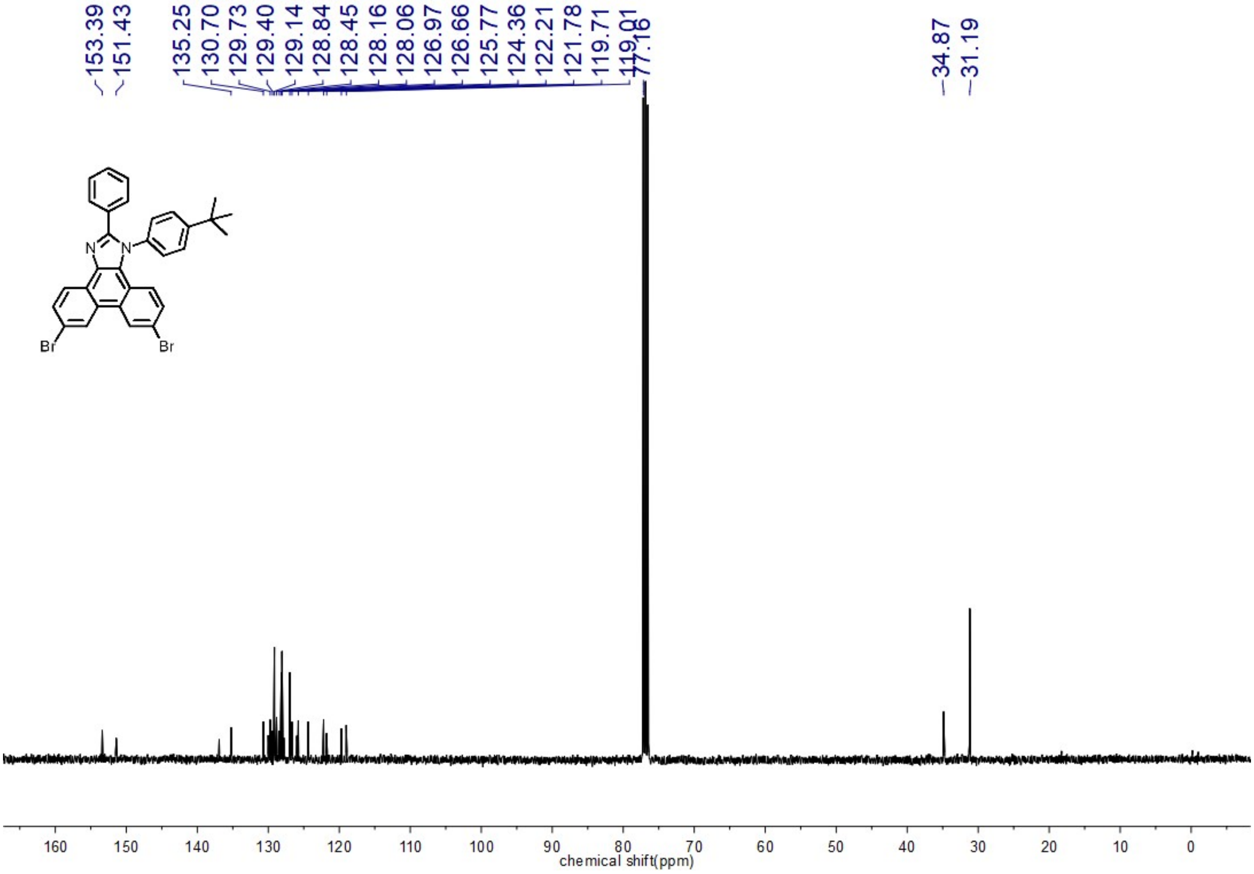

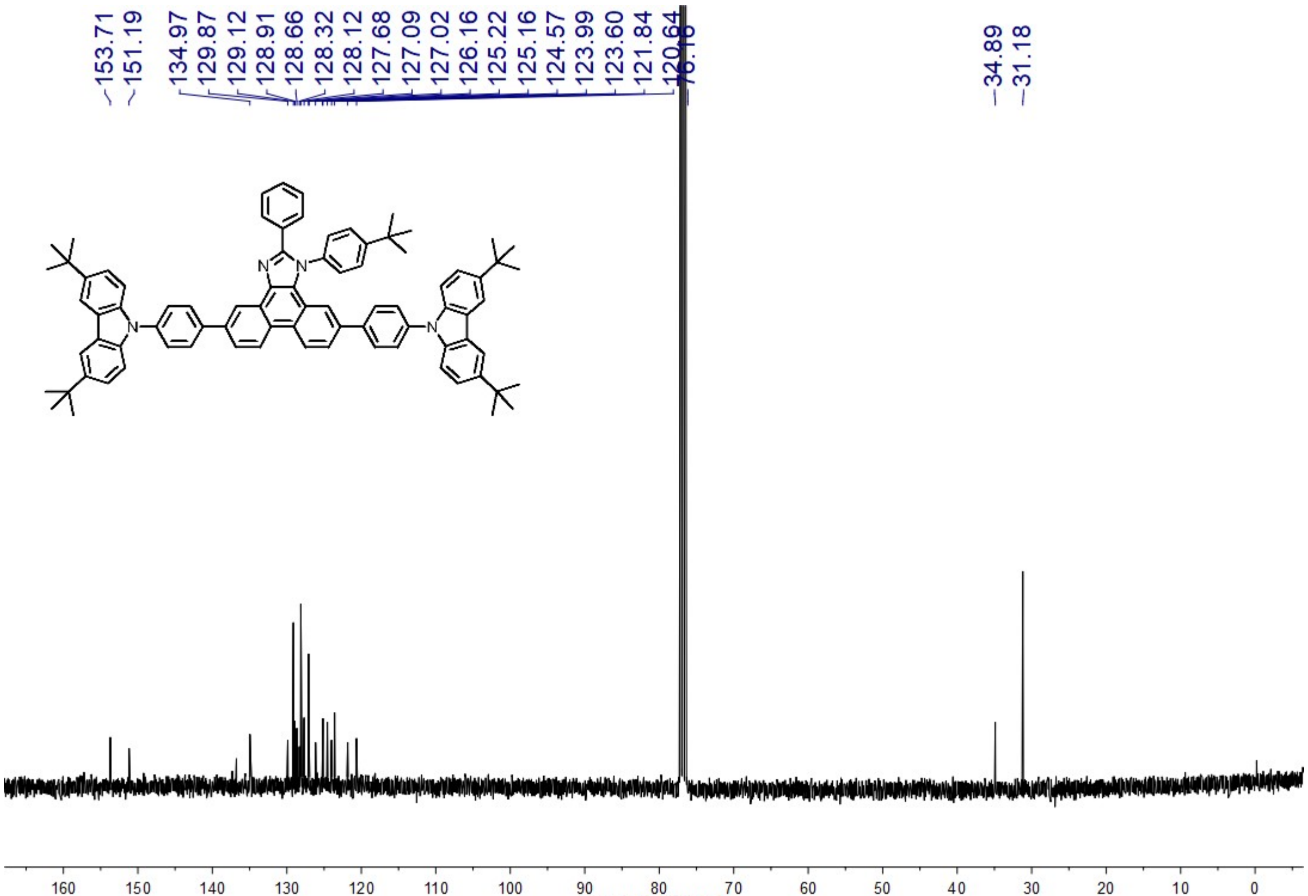
153.71
151.19
134.97
129.87
129.12
128.91
128.66
128.32
128.12
127.68
127.09
127.02
126.16
125.22
125.16
124.57
123.99
123.60
121.84
120.64
76.16
34.89
31.18
N
N
N
N
160
150
140
130
120
110
100
90
80
70
60
50
40
30
20
10
0
chemical shift(ppm)

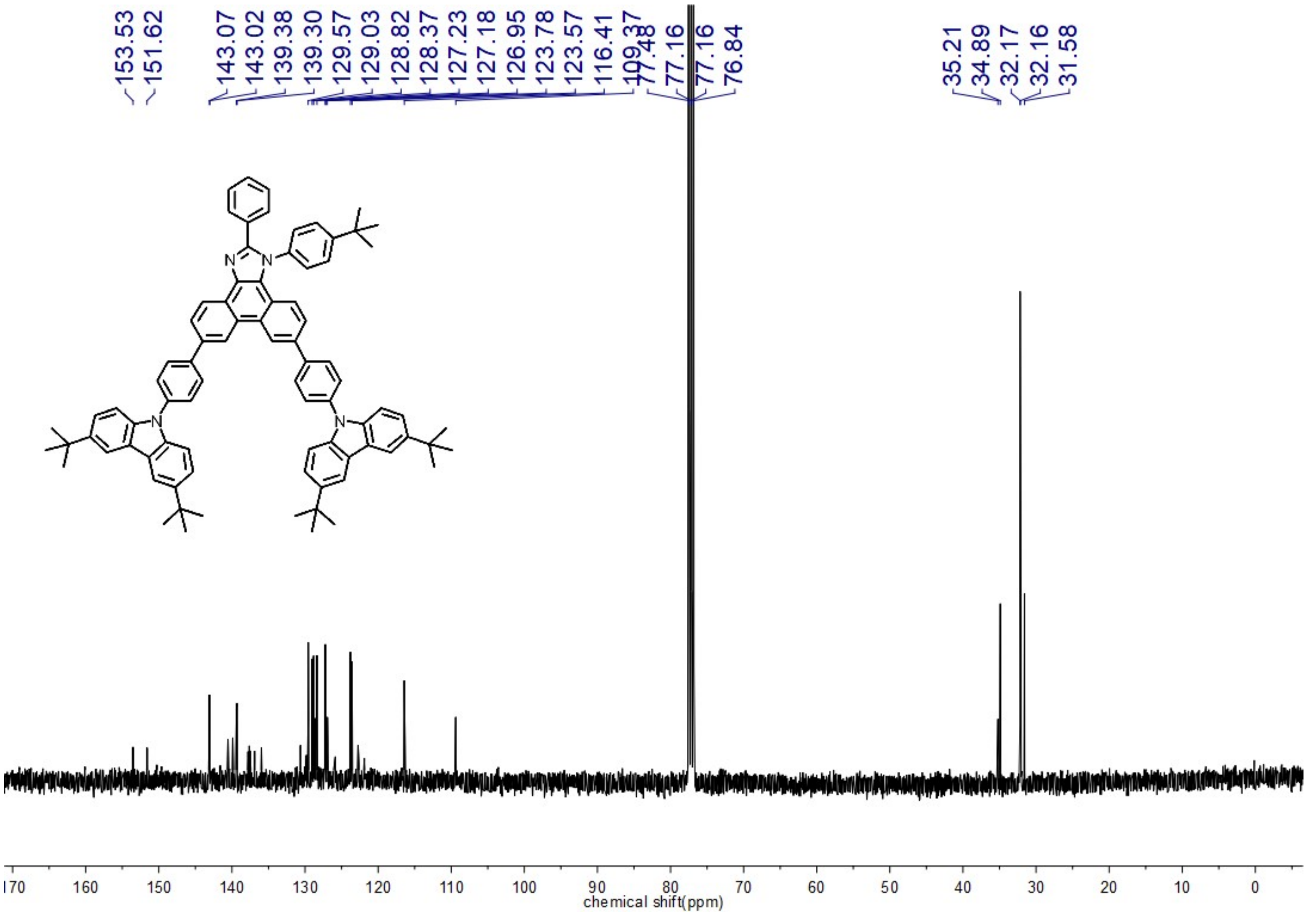
153.53
151.62
143.07
143.02
139.38
139.30
129.57
129.03
128.82
128.37
127.23
127.18
126.95
123.78
123.57
116.41
109.37
77.48
77.16
77.16
76.84
35.21
34.89
32.17
32.16
31.58
N
N
N
N
170
160
150
140
130
120
110
100
90
80
70
60
50
40
30
20
10
0
chemical shift(ppm)

V. **HR-MS** spectra of target molecules.

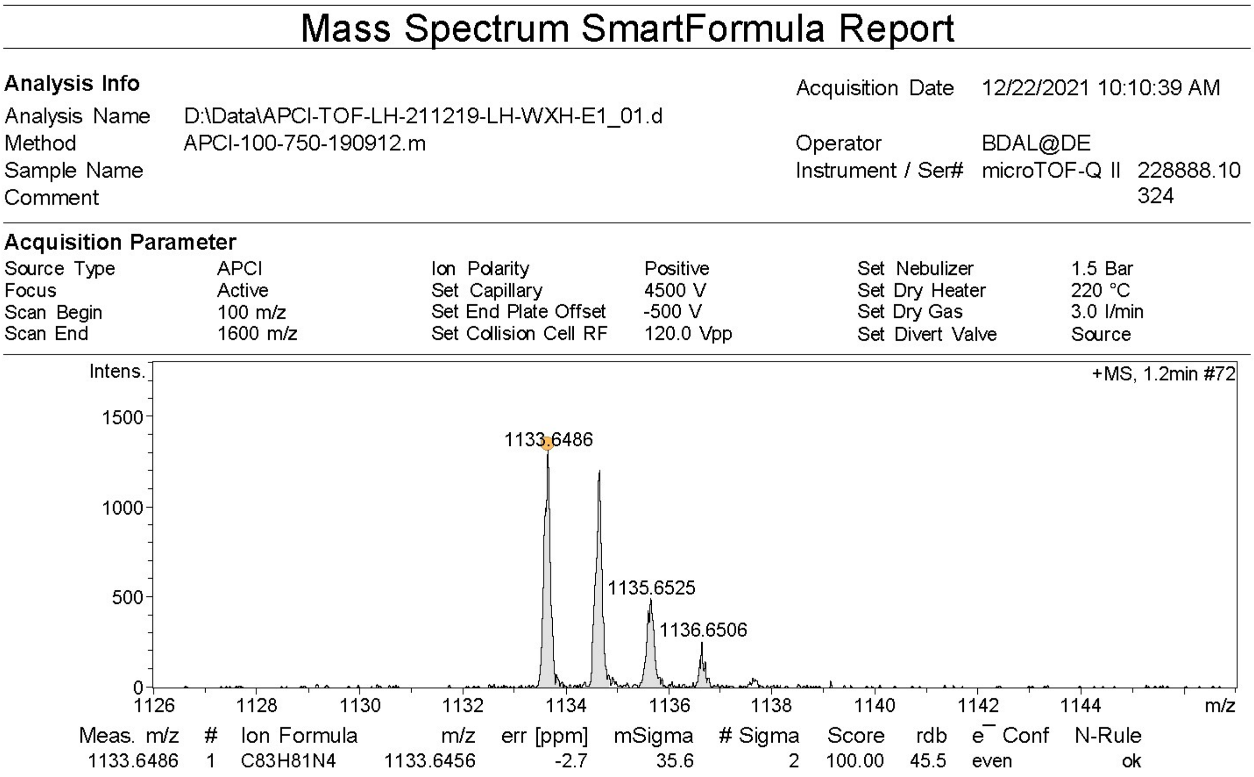

Mass Spectrum SmartFormula Report

Analysis Info

Analysis Name D:\Data\APCI-TOF-LH-211219-LH-WXH-E1_01.d
Method APCI-100-750-190912.m
Sample Name
Comment

Acquisition Date 12/22/2021 10:10:39 AM
Operator BDAL@DE
Instrument / Ser# microTOF-Q II 228888.10324

Acquisition Parameter

Source Type	APCI	Ion Polarity	Positive	Set Nebulizer	1.5 Bar
Focus	Active	Set Capillary	4500 V	Set Dry Heater	220 °C
Scan Begin	100 m/z	Set End Plate Offset	-500 V	Set Dry Gas	3.0 l/min
Scan End	1600 m/z	Set Collision Cell RF	120.0 Vpp	Set Divert Valve	Source

Meas. m/z	#	Ion Formula	m/z	err [ppm]	mSigma	# Sigma	Score	rdb	e⁻ Conf	N-Rule
1133.6486	1	C83H81N4	1133.6456	-2.7	35.6	2	100.00	45.5	even	ok

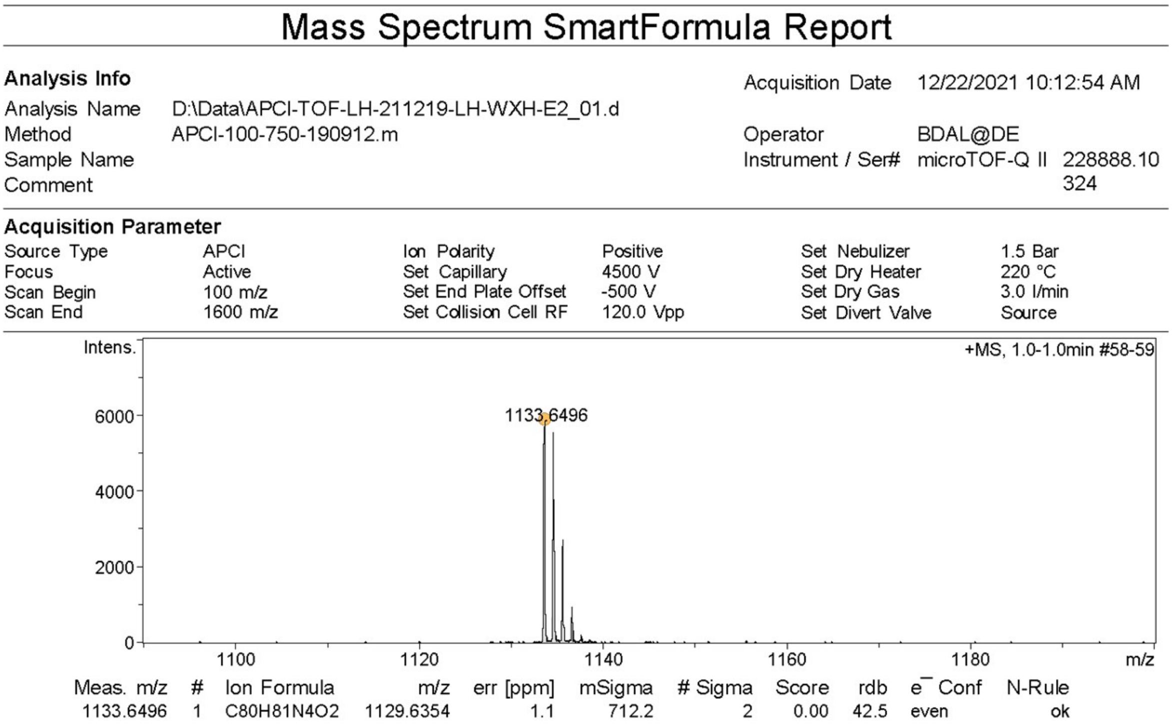

Mass Spectrum SmartFormula Report

Analysis Info

Analysis Name D:\Data\APCI-TOF-LH-211219-LH-WXH-E2_01.d
Method APCI-100-750-190912.m
Sample Name
Comment

Acquisition Date 12/22/2021 10:12:54 AM
Operator BDAL@DE
Instrument / Ser# microTOF-Q II 228888.10324

Acquisition Parameter

Source Type	APCI	Ion Polarity	Positive	Set Nebulizer	1.5 Bar
Focus	Active	Set Capillary	4500 V	Set Dry Heater	220 °C
Scan Begin	100 m/z	Set End Plate Offset	-500 V	Set Dry Gas	3.0 l/min
Scan End	1600 m/z	Set Collision Cell RF	120.0 Vpp	Set Divert Valve	Source

Meas. m/z	#	Ion Formula	m/z	err [ppm]	mSigma	# Sigma	Score	rdb	e⁻ Conf	N-Rule
1133.6496	1	C80H81N4O2	1129.6354	1.1	712.2	2	0.00	42.5	even	ok